

# A Preparation Nonstationarity Loophole in Superconducting-Qubit Bell Tests

Prosanta Pal,<sup>1</sup> Shubhanshu Karoliya,<sup>2</sup> Gargee Sharma,<sup>3</sup> and Ramakrishna Podila<sup>1</sup>

<sup>1</sup>*Department of Physics and Astronomy, Clemson University, Clemson, SC, USA*

<sup>2</sup>*Indian Institute of Technology Mandi, Mandi, H.P. 175005, India*

<sup>3</sup>*Indian Institute of Technology Delhi, Hauz Khas, New Delhi 110016, India*

(Dated: January 14, 2026)

Bell or Clauser–Horne–Shimony–Holt (CHSH) tests on superconducting quantum processors are commonly interpreted under the assumption that repeated circuit executions sample a single, stationary preparation ensemble. Here we show that this assumption can be violated on contemporary hardware, with direct implications for the interpretation of observed Bell violations. We introduce an ensemble-divergence framework in which slow temporal drift of the preparation process induces context-dependent effective ensembles, even when measurement independence and locality are preserved. This leads to a relaxed Bell bound  $|S| \leq 2 + 6\delta_{\text{ens}}$ , where  $\delta_{\text{ens}}$  quantifies preparation nonstationarity. Because  $\delta_{\text{ens}}$  is not directly observable, we develop an operational witness  $\delta_{\text{op}}$  based on bin-resolved outcome statistics for fixed measurement channels. Using Pauli-axis measurements on IBM superconducting processors, we observe statistically significant operational drift that persists after full two-qubit readout mitigation, ruling out measurement artifacts. In contrast, drift extracted from CHSH-optimal measurements is eliminated by mitigation, demonstrating that such settings are unsuitable for diagnosing preparation nonstationarity. We further show that the observed Bell violations imply only modest ensemble divergences, comparable in scale to those required in Hall-type measurement-dependence models, but arising here solely from preparation drift combined with experimental scheduling. Our results identify a preparation-dependent loophole relevant to Bell tests on noisy intermediate-scale quantum devices and highlight the necessity of drift-aware protocols for reliable quantum certification.

## I. INTRODUCTION

Superconducting-qubit processors have rapidly progressed from proof-of-concept devices to mature experimental platforms for quantum algorithms, noise characterization, and foundational tests of quantum mechanics [1–10]. Improvements in gate fidelity, scalable control electronics, and coherent multi-qubit operation have positioned superconducting circuits as leading candidates for both near-term quantum advantage demonstrations and precision tests of quantum correlations [11, 12]. Operationally, experiments on these platforms consist of repeated executions of a prepare–evolve–measure cycle, with each shot comprising state preparation, coherent control, and projective measurement [13, 14]. Most theoretical analyses and experimental interpretations implicitly assume that these repetitions sample a single, stationary preparation process, often modeled as an independent and identically distributed (i.i.d.) completely positive trace-preserving (CPTP) map acting identically on every shot [14]. Noise-modeling frameworks such as Qiskit Aer adopt this assumption explicitly, using backend-calibrated stationary CPTP channels to describe repeated executions [15].

A growing body of experimental work, however, has established that this i.i.d. assumption is frequently violated on superconducting hardware. Observed deviations include slow temporal drift, context-dependent responses, and correlated errors in state preparation and readout [16–27]. These effects arise primarily from low-frequency fluctuations in classical control parameters, such as microwave amplitudes and phases, mixer imbalances, dc offsets, flux noise, and residual qubit detunings, that introduce slowly varying imperfections into the quantum process. In multi-qubit architectures, shared-control crosstalk and calibration drift can further induce context dependence, whereby nominally identical operations exhibit small

but systematic biases that depend on circuit structure or measurement basis [23–27]. As a result, repeated executions effectively sample from an ensemble of slowly evolving preparation maps rather than a single stationary one, leading to nonstationary outcome statistics [17, 18, 27–30].

While nonstationarity and context dependence are well documented, their implications for Bell-type tests on superconducting hardware remain insufficiently explored. In the standard Bell or Clauser–Horne–Shimony–Holt (CHSH) framework [31–33], the classical bound  $|S| \leq 2$  relies on two key assumptions: locality and a single, context-independent hidden-variable distribution  $\pi(\lambda)$  underlying all correlators. Relaxing either assumption can increase the maximal attainable value of  $S$ . Hall [34] formalized one such relaxation by allowing correlations between the hidden variable and the measurement settings, quantified by a measurement-dependence parameter  $M$ . In this framework, modest measurement dependence ( $M \gtrsim 14\%$ ) suffices for local models to reproduce the quantum value  $|S| = 2\sqrt{2}$ , yielding a relaxed bound  $|S| \leq 2 + 3M$ , with subsequent refinements [35–38]. Hall’s parameter probes violations of measurement independence and is often interpreted in terms of signaling or correlations between hidden variables and setting choices.

In this work, we develop a different mechanism that relaxes the assumption of preparation stationarity. On superconducting processors, slow temporal variation of control parameters can cause the effective preparation ensemble to change over the duration of a Bell experiment. Because different CHSH settings may be executed at systematically different times, the corresponding correlators can sample distinct preparation ensembles even when the setting choices themselves remain free and random. We formalize this by introducing ensemble divergence  $\delta_{\text{ens}}$ , by defining it to be the largest statistical difference between the preparation ensembles sampled by different Bell

correlators (Eq. 2). Within local hidden-variable (LHV) models with bounded outcomes, nonzero  $\delta_{\text{ens}}$  leads to a relaxed Bell inequality  $|S| \leq 2 + 6\delta_{\text{ens}}$ , even in the absence of signaling or measurement dependence. Because the underlying preparation ensemble is not an observable, preparation nonstationarity is assessed at the level of observable statistics. We introduce an operational drift parameter  $\delta_{\text{op}}$  which quantifies the maximal change in outcome distributions observed for a fixed measurement context across different temporal subsets of an experiment. A nonvanishing  $\delta_{\text{op}}$  signals the presence of preparation nonstationarity, i.e.,  $\delta_{\text{ens}} > 0$  within LHV models, even though it does not quantify the divergence between different contexts. In Bell–CHSH experiments, nonuniform execution schedules can convert such purely temporal drift into apparent context dependence by assigning different correlators to different temporal windows.

We experimentally demonstrate how preparation nonstationarity gives rise to apparent violations of the standard CHSH bound under realistic execution conditions on IBM quantum computers. Our aim is not to survey or characterize this effect across all qubit pairs, but to establish its existence as a distinct mechanism by which Bell inequalities can be affected, independent of previously studied relaxations such as measurement dependence. To this end, we perform CHSH experiments with controlled scheduling protocols on IBM superconducting quantum processors (`ibm_fez` and `ibm_torino`). We diagnose preparation nonstationarity using Pauli-axis measurements that define fixed, time-independent classical channels, and compare the results with matched Monte Carlo (MC) null models and noise-calibrated simulations. We then examine how the independently observed preparation drift constrains the interpretation of Bell violations obtained from CHSH-optimal measurements. Our results demonstrate that Bell violations on contemporary superconducting hardware can coexist with a breakdown of the preparation-stationarity premise, opening a preparation-dependent loophole that is logically distinct from Hall-type measurement dependence.

## II. METHODS

### A. Ensemble-conditioned CHSH bounds

In the standard Bell–CHSH framework [31, 39], the four measurement contexts  $(a, b) \in \{(x, y), (x', y), (x, y'), (x', y')\}$  are assumed to probe a single, stationary preparation ensemble described by a setting-independent hidden-variable distribution  $\pi(\lambda)$ . Together with measurement independence, the assumption that the setting choices are statistically uncorrelated with  $\lambda$ , this stationarity underlies the derivation of the classical bound  $|S| \leq 2$ .

Hall [34] investigated a controlled relaxation of measurement independence by allowing correlations between the hidden variable and the measurement settings. In this approach, one permits correlations between the hidden variable  $\lambda$  and the measurement settings  $(a, b)$ , so that the conditional distribution  $p(\lambda|a, b)$  differs from the unconditional distribution  $p(\lambda)$ ; equivalently, the joint distribution fails to factorize as

$p(\lambda, a, b) = p(\lambda)p(a, b)$ , or  $p(a, b|\lambda) \neq p(a, b)$ . The degree of measurement dependence is quantified by a parameter  $M$ , defined as the maximum  $d_{\text{TV}}$  between the setting-conditioned distributions  $p(\lambda|a, b)$ , leading to the relaxed bound  $|S| \leq 2 + 3M$ . Subsequent work has derived tight inequalities and information-theoretic characterizations within this framework [35–37, 40]. These analyses exclusively concern correlations of the form  $p(a, b|\lambda)$ .

The mechanism considered here relaxes a different assumption. We maintain measurement independence in the operational sense,  $p(a, b|\lambda) = p(a, b)$ , and introduce no correlation between the hidden variables and the setting choices. Instead, we relax the assumption of preparation stationarity. In superconducting quantum processors, slow temporal variation of control parameters can cause the effective preparation ensemble to change over the duration of a Bell experiment. Since different setting pairs may be executed at systematically different times, the corresponding correlators can sample distinct preparation ensembles even when the setting choices remain free and random.

Accordingly, the correlator for a given setting pair  $(a, b)$  is described by

$$E_{ab} = \int d\lambda \pi_{ab}(\lambda) A(a, \lambda) B(b, \lambda), \quad (1)$$

where  $\pi_{ab}(\lambda)$  denotes the hidden-variable distribution associated with the preparation ensemble during the subset of runs in which  $(a, b)$  is implemented. To quantify deviations from ensemble stationarity, we define the ensemble divergence

$$\delta_{\text{ens}} = \max_{(a, b), (a', b')} d_{\text{TV}}(\pi_{ab}, \pi_{a'b'}), \quad (2)$$

with  $d_{\text{TV}}(\mu, \nu) = \frac{1}{2} \int d\lambda |\mu(\lambda) - \nu(\lambda)|$ .

We stress that  $\pi_{ab}(\lambda)$  should not be interpreted as a conditional distribution  $p(\lambda|a, b)$  in the sense of Hall [34]. Rather, it represents an effective description of preparation statistics associated with different temporal subsets of the experiment. Consequently, the parameter  $\delta_{\text{ens}}$  quantifies a breakdown of preparation stationarity, not a limitation of freedom of choice. It therefore relaxes a logically distinct assumption of the CHSH derivation from Hall’s measurement-dependence parameter  $M$ , and the two quantities are not directly interchangeable.

The effect of  $\delta_{\text{ens}}$  on the Bell parameter can be bounded within a local hidden-variable model with  $|A(a, \lambda)|, |B(b, \lambda)| \leq 1$ . Writing  $X_{ab}(\lambda) := A(a, \lambda)B(b, \lambda)$  and choosing a reference ensemble  $\pi(\lambda) \equiv \pi_{xy}(\lambda)$ , we decompose

$$E_{ab} = \int d\lambda \pi_{ab}(\lambda) X_{ab}(\lambda) \quad (3)$$

$$= \int d\lambda \pi(\lambda) X_{ab}(\lambda) + \int d\lambda [\pi_{ab}(\lambda) - \pi(\lambda)] X_{ab}(\lambda) \quad (4)$$

$$\equiv E_{ab}^{(0)} + \Delta E_{ab}. \quad (5)$$

Inserting Eqs. (5) into  $S = E_{xy} + E_{xy'} + E_{x'y} - E_{x'y'}$  and using  $\Delta E_{xy} = 0$  by construction yields  $S = S_0 + \Delta S$  with a

“reference” contribution  $S_0 = E_{xy}^{(0)} + E_{xy'}^{(0)} + E_{x'y}^{(0)} - E_{x'y'}^{(0)}$ . For each  $\lambda$  the deterministic combination  $X_{xy} + X_{xy'} + X_{x'y} - X_{x'y'}$  has magnitude at most 2, so the standard CHSH argument gives  $|S_0| \leq 2$ .

For the correction terms we use  $|X_{ab}(\lambda)| \leq 1$  and the definition of  $d_{\text{TV}}$ :

$$|\Delta E_{ab}| = \left| \int d\lambda [\pi_{ab}(\lambda) - \pi(\lambda)] X_{ab}(\lambda) \right| \quad (6)$$

$$\leq \int d\lambda |\pi_{ab}(\lambda) - \pi(\lambda)| = 2 d_{\text{TV}}(\pi_{ab}, \pi). \quad (7)$$

By Eq. (2),  $d_{\text{TV}}(\pi_{ab}, \pi) \leq \delta_{\text{ens}}$  for all  $(a, b)$ , so  $|\Delta E_{ab}| \leq 2\delta_{\text{ens}}$  for the three nonreference contexts  $(xy', x'y, x'y')$ . Hence

$$|\Delta S| \leq |\Delta E_{xy'}| + |\Delta E_{x'y}| + |\Delta E_{x'y'}| \leq 6\delta_{\text{ens}}, \quad (8)$$

and we obtain the relaxed CHSH inequality

$$|S| \leq |S_0| + |\Delta S| \leq 2 + 6\delta_{\text{ens}}. \quad (9)$$

Equation (9) shows that the variation of preparation ensembles alone can increase the maximal Bell parameter by an amount proportional to  $\delta_{\text{ens}}$ , without relaxing locality or freedom-of-choice assumptions. In particular, a violation  $|S| > 2$  implies  $\delta_{\text{ens}} \geq (|S| - 2)/6$  for any local hidden-variable model with deterministic or bounded outcomes.

## B. Operational ensemble drift

The ensemble divergence  $\delta_{\text{ens}}$  defined in Eq. (2) characterizes variability of the hidden preparation ensembles  $\pi_{ab}(\lambda)$  across temporal bins used in experiments. Because  $\pi_{ab}$  is not directly observable, we assess nonstationarity at the level of the operational outcome statistics. For a fixed context  $(a, b)$ , let  $p_{ab}^{(i)}(x)$  denote the empirical distribution over bitstrings in time bin  $i$ . We define the operational ensemble drift

$$\delta_{\text{op}}(ab) = \max_{i < j} d_{\text{TV}}(p_{ab}^{(i)}, p_{ab}^{(j)}), \quad \delta_{\text{op}}^{\text{global}} = \max_{(a, b)} \delta_{\text{op}}(ab), \quad (10)$$

which quantifies the maximal variation of the observed statistics for a single measurement channel. Since each context induces a fixed classical map  $\pi_{ab} \mapsto p_{ab}$ , the contractivity of TV distance implies

$$\delta_{\text{op}}(ab) \leq d_{\text{TV}}(\pi_{ab}^{(i)}, \pi_{ab}^{(j)}) \leq \delta_{\text{ens}}, \quad (11)$$

so any nonzero operational drift certifies  $\delta_{\text{ens}} > 0$ . However, because different CHSH settings correspond to distinct measurement channels, Eq. (11) does not extend across settings. Consequently,  $\delta_{\text{op}}$  provides a valid witness of preparation nonstationarity but does not quantify the magnitude of  $\delta_{\text{ens}}$  or its variation between contexts.

An additional operational issue concerns the choice of measurement bases used to evaluate  $\delta_{\text{op}}$ . While CHSH-optimal settings (measurement axes in the  $XZ$  plane separated by angles  $\{0, \frac{\pi}{2}\}$  on one qubit and  $\{\pm \frac{\pi}{4}\}$  on the other) maximize the

Bell violation [41, 42], they correspond to non-orthogonal, continuously calibrated measurement axes. Slow drift in control amplitudes, phases, or qubit frequencies can therefore induce basis-dependent mixing of outcome probabilities, making it difficult to distinguish genuine preparation nonstationarity from measurement-axis drift at the level of raw statistics [43]. For this reason, we evaluate  $\delta_{\text{op}}$  using fixed Pauli  $X, Y, Z$  measurement axes. Pauli measurements define orthogonal, time-independent classical channels whose outcome probabilities are directly interpretable and stable under small coherent control errors. This choice aligns with IBM Quantum calibration protocols, in which Pauli measurements are routinely calibrated and monitored as fixed reference bases. Consequently, variations of  $p_{ab}^{(i)}$  across temporal bins can be attributed conservatively to changes in the effective preparation ensemble rather than to measurement-channel drift.

## C. Qiskit-Aer simulations with real backend noise

To select an appropriate temporal binning for the hardware experiments, we performed forward simulations using Qiskit Aer with noise models calibrated from each backend at the time of data acquisition. These simulations are not intended to reproduce the experimental data quantitatively, but rather to assess how operational measures of preparation nonstationarity respond to realistic levels of slow drift under controlled conditions.

*Measurement settings.* In these simulations, we implement the CHSH measurement contexts by performing projective measurements of each qubit in the singlet state along specified Pauli axes. The four contexts  $(X, Y)$ ,  $(X, Z)$ ,  $(Z, Y)$ , and  $(Z, Z)$  correspond to joint measurements of the observables  $\sigma_X^A \otimes \sigma_Y^B$ ,  $\sigma_X^A \otimes \sigma_Z^B$ ,  $\sigma_Z^A \otimes \sigma_Y^B$ , and  $\sigma_Z^A \otimes \sigma_Z^B$ , respectively. Operationally, these measurements are implemented by applying single-qubit rotations that map the chosen Pauli basis onto the computational basis, followed by standard projective measurement in the  $Z$  basis on both qubits. As discussed earlier, these settings are chosen to avoid conflating drift-induced nonstationarity with angle-dependent sensitivity amplification that arises for optimal CHSH settings.

*Drift model.* To emulate experimentally realistic nonstationarity, we augment the real backend Aer noise model with a weak, coherent drift applied at the state-preparation level. Specifically, for each temporal bin  $b \in \{1, \dots, B\}$  and each CHSH context, both qubits undergo small phase rotations

$$U_{\text{drift}}^{(b)} = \exp[-i\theta_b Z_a] \exp[i\theta_b Z_b], \quad (12)$$

where  $\theta_b$  varies smoothly across the acquisition window. In the simulations presented here,  $\theta_b$  is swept linearly from  $-\theta_{\text{max}}$  to  $+\theta_{\text{max}}$  across all bins and contexts, mimicking slow calibration drift or control-parameter wander on timescales longer than a single bin but shorter than the full experiment. We consider  $\theta_{\text{max}} \in \{0, 10^{-2}, 10^{-1}\}$ , corresponding to bin-to-bin probability variations ranging from purely statistical fluctuations to percent-level changes comparable to those observed in preliminary hardware runs.

*Scheduling protocols.* Two execution schedules are simulated: an interleaved (round-robin) schedule, where all four contexts are sampled within each bin, and an unbalanced (blocked) schedule, where all bins of a given context are executed contiguously. Both schedules use identical total shot counts (1024 shots per bin) and drift profiles, differing only in how drift is mapped onto measurement contexts. This allows us to disentangle drift-induced ensemble variation from trivial shot-count effects.

*Bin-number scan and null model.* For each backend and drift strength, we scan the number of bins  $B \in \{3, 6, 9, 12\}$  while keeping the number of shots *per bin* fixed at 1024. As a result, the total number of shots per context scales linearly with  $B$ . For each configuration, we compute the operational ensemble divergence  $\delta_{\text{op}}$  as the maximum  $d_{TV}$  between empirical outcome distributions drawn from different bins. To assess whether the observed  $\delta_{\text{op}}$  exceeds what is expected from finite sampling alone, we construct a MC null distribution by resampling i.i.d. multinomial data with the same number of bins and shots per bin as in the simulated experiment. Importantly, because the shots per bin are held fixed, increasing  $B$  does not simply sharpen statistical resolution; it also inflates the null distribution of  $\delta_{\text{op}}$  through extreme-value statistics. As a result, the comparison between observed and null values should not be interpreted as a hypothesis test in the conventional sense. Rather, it provides an operational diagnostic of the regime in which drift-induced ensemble variation becomes distinguishable from finite-sample fluctuations under experimentally realistic constraints.

#### D. Hardware experiments on superconducting quantum processors

*CHSH measurements along Pauli axes.* Hardware experiments are performed using the same binning, scheduling, and statistical analysis protocols as those established in the Qiskit-Aer simulations (Sec. II C), with the sole difference that all circuits are executed on real IBM superconducting quantum processors and no explicit drift is introduced. We prepared the singlet state  $|\Psi^-\rangle = (|01\rangle - |10\rangle)/\sqrt{2}$  on connected qubit pairs ((40, 41) on `ibm_torino` and (0, 1) on `ibm_fez`) using standard Hadamard–CNOT sequences followed by local phase adjustments.

Our objective is to demonstrate the existence of a preparation nonstationarity loophole under realistic experimental conditions, rather than to establish its prevalence across all qubit pairs or devices. Accordingly, we do not attempt an exhaustive survey. We performed CHSH tests on multiple candidate qubit pairs across the two backends ((0, 1), (2, 3), and (40, 41) on `ibm_torino` and (0, 1), (25, 37), (34, 35), (37, 45), and (140, 141) on `ibm_fez`), but restricted the more time-intensive  $\delta_{\text{op}}$  measurements to two representative pairs due to the substantial cost ( $\sim 96$  s wall-clock time per pair for combined round-robin and unbalanced schedules with  $B = 6$  bins). These candidate pairs were screened a priori using publicly available calibration data (including readout error, two-qubit gate error, and  $T_1/T_2$  variability) together with short

pilot runs to identify pairs with elevated temporal variability.

On all hardware runs, data acquisition is divided into  $B = 6$  temporal bins with 1024 shots per bin per context, and both round-robin and unbalanced execution schedules are employed to map temporal variation onto measurement contexts. Measurements are performed using fixed Pauli axes  $(X, Y)$ ,  $(X, Z)$ ,  $(Z, Y)$ , and  $(Z, Z)$ , implemented via single-qubit basis rotations followed by projective measurement in the computational basis. While Pauli measurements are often treated operationally as defining time-independent classical channels, we note that on superconducting qubits they are realized through pre-rotations and therefore inherit any residual instability in single-qubit control [44, 45]. This effect must be distinguished from preparation nonstationarity and explicitly controlled. As discussed later in Sec. III A, we address this by bounding the stability of the relevant single-qubit rotations over the acquisition window and by verifying that their contribution is parametrically smaller than the observed bin-to-bin variations. With this control in place, the use of Pauli axes avoids conflating preparation nonstationarity with the basis-dependent sensitivity inherent to CHSH-optimal settings. Operational ensemble drift  $\delta_{\text{op}}$  is computed from the bin-resolved outcome distributions exactly as in the simulations, and its statistical significance is assessed using a MC null constructed with the same number of bins and shots per bin.

*CHSH measurements along optimal axes.* In addition to Pauli-axis measurements used to diagnose preparation nonstationarity, we perform standard CHSH tests using measurement settings that maximize the quantum violation for a singlet state. Specifically, each qubit is measured along axes in the  $X - Z$  plane defined by angles  $\theta$  with respect to  $Z$ , with settings  $\theta_A \in \{0, \pi/2\}$  for qubit A and  $\theta_B \in \{\pm\pi/4\}$  for qubit B. These correspond to the canonical CHSH-optimal choices yielding  $|S| = 2\sqrt{2}$  for an ideal singlet. Operationally, a measurement along angle  $\theta$  is implemented by a single  $R_Y(-\theta)$  rotation followed by projective measurement in the computational basis. For each qubit pair and backend ((40, 41) on `ibm_torino` and (0, 1) on `ibm_fez`), we prepare the singlet state  $|\psi^-\rangle = (|01\rangle - |10\rangle)/\sqrt{2}$  and evaluate the four correlators entering the CHSH parameter  $S$ . Two scheduling protocols are employed: a round-robin schedule, in which all four settings are executed within each repeat, and an unbalanced (or blocked) schedule, in which each setting is executed contiguously across repeats. Each correlator is estimated from 1024 shots per circuit, and  $S$  is computed solely from counts aggregated over all repeats for a given setting. We emphasize that these CHSH-optimal measurements are used exclusively to estimate Bell violations. Because the corresponding measurement channels depend on continuously calibrated analog rotation angles, they are not used to extract  $\delta_{\text{op}}$ , as slow basis drift can mimic preparation nonstationarity at the level of outcome statistics.

*Two-qubit readout mitigation.* To reduce state-preparation-and-measurement (SPAM) bias in both the aggregated CHSH estimator and the bin-resolved drift statistics, we apply classical measurement-error mitigation based on an empirically calibrated two-qubit assignment matrix  $M \in \mathbb{R}^{4 \times 4}$ . Here SPAM refers to deviations

between the intended preparation/measurement procedure and the realized classical readout statistics, which can systematically distort the observed outcome frequencies. For each backend and physical qubit pair, the matrix elements are defined as  $M_{x,y} = P(\text{meas} = x \mid \text{prep} = y)$  with  $x, y \in \{00, 01, 10, 11\}$ , and are obtained by preparing each computational basis state  $|y\rangle$  and estimating the resulting outcome distribution over  $x$ . Calibrating a single joint channel on the two-qubit outcome space captures correlated assignment effects and leakage between outcomes that may not be represented by single-qubit figures of merit or separable models—a point emphasized by recent analyses of multiplexed readout quality beyond assignment fidelity [46]. Mitigated distributions are obtained by linear inversion,  $\hat{p}^{\text{mit}} = M^{-1}\hat{p}$ , with conditioning checks and renormalization to the probability simplex to limit noise amplification [47–49]. Unlike linear inversion, more sophisticated mitigation strategies based on Bayesian inference or full POVM reconstruction can incorporate additional assumptions or priors that may adapt to statistical fluctuations and partially absorb time-dependent effects into the inference itself [49, 50]. Such adaptivity, while advantageous for state estimation, would obscure the drift signatures we seek to quantify. For this reason, we adopt linear inversion with standard numerical safeguards as a conservative and operationally well-defined procedure for isolating preparation nonstationarity. Importantly, we apply the same mitigation procedure independently to each temporal bin prior to computing  $\delta_{\text{op}}$ , so that the drift diagnostic compares bin-to-bin variations in inferred pre-assignment statistics rather than raw readout artifacts.

### III. RESULTS

#### A. Operational ensemble drift along Pauli axes

Figure 1 shows the global operational drift  $\delta_{\text{op}}^{\text{global}}$  [Eq. (10)] extracted from Pauli-basis measurements in noise-calibrated simulations as a function of the number of temporal bins  $B$ , execution schedule, and imposed drift amplitude, together with a matched MC null. In the absence of drift ( $\theta_{\text{max}} = 0$ ), the observed  $\delta_{\text{op}}^{\text{global}}$  follows the null for all  $B$ , with the weak increase reflecting extreme-value broadening rather than physical nonstationarity. At intermediate drift ( $\theta_{\text{max}} = 10^{-2}$ ), deviations from the null become marginally resolvable, with the first consistent separation appearing at  $B \approx 6$ , particularly under unbalanced scheduling. For larger drift ( $\theta_{\text{max}} = 10^{-1}$ ), the observed  $\delta_{\text{op}}$  saturates for  $B \gtrsim 6$ , indicating diminishing returns from further binning while the null continues to broaden. Thus,  $B = 6$  represents the minimal binning that resolves drift-induced nonstationarity without incurring unnecessary statistical inflation or shot overhead. Identifying this minimal binning is operationally important. On real IBM QPUs, increasing  $B$  increases total circuit executions without improving sensitivity, directly inflating experimental cost. Moreover, larger  $B$  increases the likelihood that bins are executed at widely separated wall-clock times due to queueing and priority scheduling, introducing additional uncontrolled

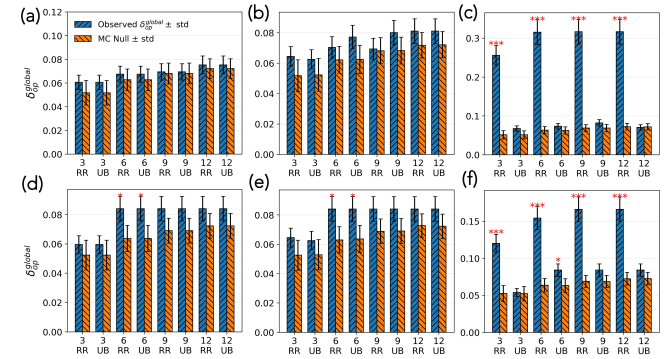


FIG. 1. Operational ensemble drift  $\delta_{\text{op}}^{\text{global}}$  extracted from Monte-Carlo-simulated CHSH experiments under controlled preparation drift. Panels (a)–(c) correspond to the `ibm_fez` backend using qubit pair (0,1), while panels (d)–(f) correspond to the `ibm_torino` backend using qubit pair (40,41). Vertically aligned panels share the same drift amplitude: (a,d)  $\theta_{\text{max}} = 0$ , (b,e)  $\theta_{\text{max}} = 0.01$ , and (c,f)  $\theta_{\text{max}} = 0.1$ . For each panel, results are shown as a function of the number of temporal bins  $B$  and scheduling protocol (RR: round-robin; UB: unbalanced). Blue hatched bars denote the observed  $\delta_{\text{op}}^{\text{global}} \pm$  one standard deviation, while orange hatched bars indicate the Monte-Carlo null mean  $\pm$  one standard deviation. Red asterisks indicate statistically significant deviations from the null distribution ( $* p < 0.05$ ,  $** p < 0.01$ ,  $*** p < 10^{-3}$ ).

temporal variation. Thus,  $B = 6$  represents the smallest binning that resolves drift-induced nonstationarity while minimizing QPU overhead and avoiding artificial temporal segregation. All hardware experiments therefore use  $B = 6$ .

Figure 2 summarizes the experimentally observed operational ensemble drift  $\delta_{\text{op}}$  extracted from CHSH experiments executed on two distinct IBM superconducting quantum processors. For each device, we compare round-robin and unbalanced scheduling protocols, reporting both raw and readout-mitigated estimates of  $\delta_{\text{op}}$ , along with MC null distributions that incorporate finite-shot effects and the precise experimental scheduling structure.

The simulations (Fig. 1) establish a clear baseline expectation. In the absence of preparation nonstationarity, the simulated null distributions predict  $\delta_{\text{op}}$  values that remain confined to a narrow range set by finite-shot fluctuations, with no systematic dependence on scheduling protocol. This behavior is reflected in the null bars shown in Fig. 2, which are comparable for round-robin and unbalanced execution. For both `ibm_fez` and `ibm_torino`, the observed  $\delta_{\text{op}}$  in round-robin exceeds the simulated null by multiple standard deviations, with statistical significance ranging from  $p < 0.05$  to  $p < 10^{-3}$ . The persistence of this excess after readout mitigation rules out classical measurement errors as the dominant mechanism: if readout errors were responsible, the mitigated experimental values would collapse toward the simulated null, which is not observed. Under unbalanced scheduling, the experimentally observed  $\delta_{\text{op}}$  is substantially reduced for `ibm_fez` and becomes consistent with the simulated null, in quantitative agreement with simulation predictions. However, `ibm_torino` shows a significant difference even for unbalanced scheduling,

suggesting stronger nonstationarity in preparation.

To further assess whether readout mitigation could artificially induce schedule-dependent effects, we examined the conditioning of the two-qubit assignment matrix  $A$ . For both `ibm_fez` and `ibm_torino`,  $\kappa(A)$  is moderate ( $\kappa \approx 20\text{--}24$ ) and, for a given backend, indistinguishable between round-robin and unbalanced executions with identical binning and shot counts. Although small run-to-run fluctuations are observed, as expected from routine recalibration, the conditioning shows no systematic dependence on scheduling. To test the stability of readout mitigation over different bins with in each schedule, we measured  $M$  at four time points separated by six-bin blocks ( $\sim 48$  s). The condition number remains stable,  $\kappa_2(M) \approx 20\text{--}24$  across all snapshots, while the change relative to the earliest calibration is small ( $\|M_{\text{early}} - M\|_F \approx 0.02$  and  $\max_{ij} |\Delta M_{ij}| \lesssim 0.02$ ). These variations are well within the numerical stability of the inversion and show no evidence of time-dependent degradation on the scale of the experiment. This indicates that readout-matrix inversion remains numerically stable throughout the experiments and cannot account for the observed schedule-dependent behavior in the CHSH results.

Pauli-axis  $\delta_{\text{op}}$  uses fixed single-qubit rotations ( $\sqrt{X}/X$  and virtual  $R_z$ ). Calibration data nearest the runs bound single-qubit control drift to induce  $\lesssim 10^{-3}$  changes in outcome probabilities, over an order of magnitude below the observed  $\delta_{\text{op}} \approx 0.06\text{--}0.09$  under unbalanced execution (i.e., a separation of  $\gtrsim 50\times$ ). The absence of schedule dependence in these calibration metrics rules out single-qubit rotation instability as the origin of the observed  $\delta_{\text{op}}$ .

The statistically significant operational nonstationarity observed in Fig. 2 has direct implications for the interpretation of Bell tests on superconducting hardware. As shown in Sec. II A, any local hidden-variable model with ensemble divergence  $\delta_{\text{ens}} > 0$  obeys a relaxed bound  $|S| \leq 2 + 6\delta_{\text{ens}}$ . While  $\delta_{\text{ens}}$  is not directly accessible, the experimentally observed  $\delta_{\text{op}} > 0$  constitutes a verifiable witness that the assumption of a single stationary preparation ensemble, required for the standard CHSH bound, is violated. Accordingly, in regimes where  $\delta_{\text{op}}$  exceeds the finite-shot null, the strict classical bound  $|S| \leq 2$  is no longer guaranteed by the operational premises of the experiment, even in the absence of signaling or freedom-of-choice violations.

We emphasize that  $\delta_{\text{op}}$ , extracted from fixed Pauli-axis measurements, cannot be substituted into Eq. 9 to quantify Bell-bound relaxation for CHSH-optimal settings, as different contexts define distinct classical channels acting on the preparation ensemble. Accordingly, our results do not claim a quantitative explanation of the observed CHSH values in terms of Pauli-axis drift alone. Rather, the data in Fig. 2 establish a preparation-dependent loophole that is logically distinct from Hall-type measurement dependence: measurement independence is preserved, while temporal variation of the preparation ensemble sampled by different correlators relaxes the assumptions required for the standard CHSH bound. The persistence of  $\delta_{\text{op}}$  after two-qubit readout mitigation and its sensitivity to scheduling protocol indicate that this effect originates in state preparation rather than in measurement artifacts.

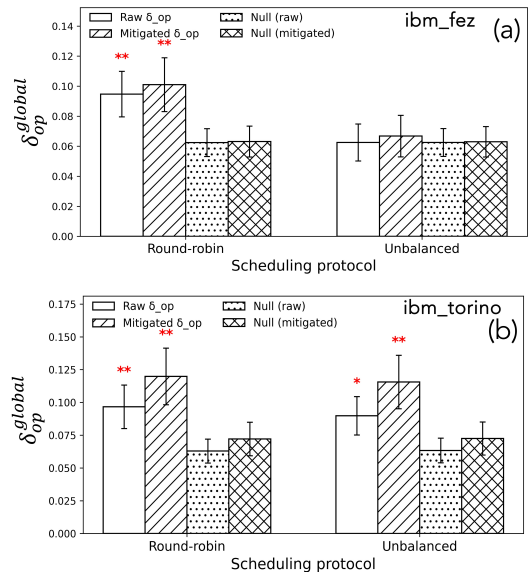


FIG. 2. Experimentally extracted operational ensemble drift  $\delta_{\text{op}}$  on (a) the `ibm_fez` backend using qubit pair (0,1) and (b) the `ibm_torino` backend using qubit pair (40,41). Results are shown for round-robin and unbalanced scheduling protocols. White and hatched blue bars denote the observed raw and readout-mitigated  $\delta_{\text{op}}$ , respectively, while dotted and cross-hatched bars indicate the corresponding Monte-Carlo null expectations constructed using identical shot budgets and scheduling structure. Error bars denote one standard deviation. Red asterisks indicate statistically significant deviations from the null (\*  $p < 0.05$ , \*\*  $p < 0.01$ ).

## B. Operational tests along optimal CHSH settings

For completeness, we also evaluate the operational drift  $\delta_{\text{op}}$  using outcome statistics obtained from CHSH-optimal measurement settings. In the raw data Fig. 3, the experimentally extracted  $\delta_{\text{op}}$  appears significantly larger than the corresponding MC null for both devices and scheduling protocols. However, after applying full two-qubit readout mitigation, the experimental values become statistically indistinguishable from the null within uncertainty. This behavior contrasts sharply with the Pauli-axis results of Fig. 2, where significant deviations persist after mitigation.

This sensitivity to mitigation reflects the fact that CHSH-optimal measurements are implemented via continuously calibrated analog rotations. Slow drift in control amplitudes, phases, or qubit frequencies can therefore induce basis-dependent mixing of outcome probabilities that mimics nonstationarity at the level of raw statistics. As a result,  $\delta_{\text{op}}$  extracted from CHSH-optimal settings conflates preparation variation with measurement-axis instability and does not provide a reliable witness of ensemble nonstationarity. For this reason, CHSH-optimal measurements are used here exclusively to estimate the Bell parameter  $S$ , while operational drift is diagnosed using fixed Pauli measurement axes.

Figure 4 shows the experimentally measured Bell parameter  $|S|$  obtained using CHSH-optimal measurement settings. As expected, readout mitigation systematically increases  $|S|$  for

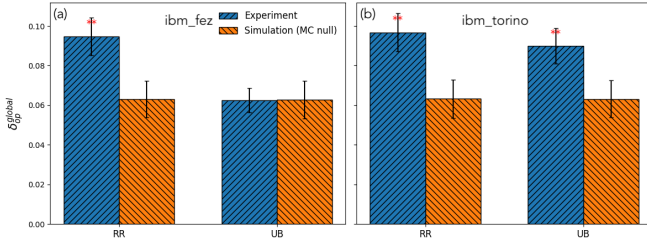


FIG. 3. Operational drift  $\delta_{op}$  extracted from outcome statistics measured along CHSH-optimal axes. Panels (a,b) show raw experimental values for `ibm_fez` (qubit pair (0,1)) and `ibm_torino` (qubit pair (40,41)), respectively, compared with matched Monte Carlo (MC) null distributions for round-robin (RR) and unbalanced (UB) scheduling. While the raw data exhibit apparent deviations from the null, these differences are eliminated by mitigation (data not shown), rendering the experimental  $\delta_{op}$  statistically consistent with the null. This behavior indicates that  $\delta_{op}$  extracted from CHSH-optimal settings is dominated by basis-dependent measurement instabilities rather than genuine preparation nonstationarity.

both devices and scheduling protocols, recovering violations of the classical bound in cases where raw data lie below  $|S| = 2$ . Viewed in isolation, these results would be interpreted as evidence of nonclassical correlations.

However, these CHSH measurements must be interpreted in light of the independently observed preparation nonstationarity reported in Fig. 2. The CHSH parameter  $S$  is estimated from statistics aggregated over all repetitions of a given measurement setting, and therefore probes only time-averaged correlators. As a result, CHSH-optimal measurements are insensitive to the temporal structure of the experiment and cannot diagnose whether different correlators sample the same underlying preparation ensemble.

Consequently, the observation of  $|S| > 2$  does not, by itself, guarantee that the assumptions required for the standard Bell–CHSH bound are satisfied. In particular, the Pauli-axis diagnostics establish that the effective preparation ensemble varies across the experiment for `ibm_fez` (round-robin) and `ibm_torino` (both schedules), implying  $\delta_{ens} > 0$ . In this regime, the relevant classical benchmark is no longer  $|S| \leq 2$ , but the relaxed bound  $|S| \leq 2 + 6\delta_{ens}$ , even though  $\delta_{ens}$  itself cannot be inferred from CHSH-optimal data.

These results therefore demonstrate a preparation-dependent loophole that persists even when measurement independence is operationally satisfied and readout errors are mitigated. Bell violations observed under such conditions cannot be interpreted as device-independent evidence against local realism without an accompanying assessment of preparation stationarity.

As an operational consistency check, we examined marginal (no-signaling) constraints in the CHSH data. For each context  $(x, y) \in \{0, 1\}^2$ , we form the one-party marginals  $P_A(a|x, y) = \sum_b P(a, b|x, y)$  and  $P_B(b|x, y) = \sum_a P(a, b|x, y)$  from the observed two-bit frequencies. Standard no-signaling requires  $P_A(a|x, y) = P_A(a|x, y')$  for fixed  $x$  and  $P_B(b|x, y) = P_B(b|x', y)$  for fixed  $y$ . We test the four corresponding comparisons using two-proportion  $z$ -tests and

TABLE I. No-signaling (marginal-consistency) summary for each device and schedule. For each dataset, four marginal-comparison tests (two for Alice and two for Bob) are performed. We report the maximum absolute deviation  $\max |\Delta P|$ , the minimum two-sided  $p$ -value  $\min p$ , and the Bonferroni-corrected minimum  $p$ -value  $\min p_{\text{Bonf}} = \min(1, 4 \min p)$ . Results are shown for raw counts and, where indicated, for readout-mitigated distributions.

Device / schedule	Version	$\max  \Delta P $	$\min p$	$\min p_{\text{Bonf}}$
<code>ibm_fez</code> (q0–1), RR	raw	0.0067	0.45	1
<code>ibm_fez</code> (q0–1), RR	mitigated	0.0093	0.32	1
<code>ibm_fez</code> (q0–1), UB	raw	0.0179	0.047	0.19
<code>ibm_fez</code> (q0–1), UB	mitigated	0.0116	0.19	0.79
<code>ibm_torino</code> (q40–41), RR	raw	0.0123	0.17	0.71
<code>ibm_torino</code> (q40–41), RR	mitigated	0.0141	0.1	0.43
<code>ibm_torino</code> (q40–41), UB	raw	0.0168	0.024	0.09
<code>ibm_torino</code> (q40–41), UB	mitigated	0.1723	$\ll 10^{-6}$	$\ll 10^{-6}$

report the maximum absolute marginal deviation  $\max |\Delta P|$ , the minimum two-sided  $p$ -value, and a Bonferroni-corrected minimum  $p$ -value (factor 4); results are summarized in Table I. Such empirical marginal tests have recently been used as operational diagnostics in superconducting-qubit Bell experiments [51].

Crucially, these marginal-consistency tests implicitly assume stationarity of the underlying preparation and measurement processes. While this assumption underlies standard interpretations of no-signaling diagnostics [51], it must be reconsidered in the presence of temporal drift. In this case, the experimentally accessible probabilities are time-averaged mixtures whose effective ensembles depend on the execution schedule. Apparent violations of marginal consistency in aggregated data therefore diagnose context-dependent sampling of a nonstationary ensemble, rather than signaling or nonlocal influence. Consistent with this interpretation, round-robin schedules, which enforce more uniform temporal sampling, exhibit suppressed marginal deviations, while unbalanced schedules show enhanced deviations. This behavior is fully compatible with instantaneous locality at the level of individual executions and does not contradict the  $\delta_{op}$  analysis, which is specifically designed to quantify operational nonstationarity across temporal bins.

### C. Schedule-aware lower bound on $\delta_{ens}$

To connect the observed Bell violations to the preparation-nonstationarity framework without identifying  $\delta_{op}$  with  $\delta_{ens}$ , we compute the minimal ensemble divergence required for a local model to accommodate a measured value of  $|S|$  using Eq. 9:  $\delta_{ens}^{\min} = (|S| - 2)/6$ . From Fig. 4, the mitigated CHSH values imply  $\delta_{ens}^{\min} \approx 0.11\text{--}0.12$  for `ibm_fez` and  $\delta_{ens}^{\min} \approx 0.03\text{--}0.04$  for `ibm_torino`. These numbers should be interpreted only as the scale of preparation divergence that would be necessary for a local explanation within our relaxed-bound analysis; they do not follow from  $\delta_{op}$ , which is channel dependent and was intentionally extracted from fixed Pauli measurements. Nevertheless, the Pauli-axis diagnostics in Fig. 2 establish  $\delta_{ens} > 0$ .

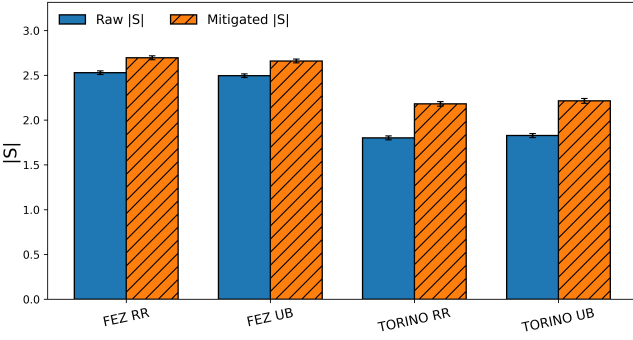


FIG. 4. Absolute Bell parameter  $|S|$  measured using CHSH-optimal settings on `ibm_fez` (qubit pair (0,1)) and `ibm_torino` (qubit pair (40,41)). Blue bars are computed from raw counts and hatched orange bars from the corresponding readout-mitigated counts, shown for round-robin (RR) and unbalanced (UB) schedules; error bars denote one standard deviation. This figure reports the standard CHSH estimator of  $S$  but does not test the preparation-stationarity assumption required for the ideal bound  $|S| \leq 2$ ; stationarity is assessed independently via the bin-resolved drift diagnostics in Fig. 2. Consequently,  $|S|$  should be interpreted jointly with Fig. 2 when assessing whether the operational premises of the standard CHSH derivation are satisfied on hardware.

operationally and provide an empirical constraint on how large preparation variation could plausibly be on hardware. In particular, the relatively small  $\delta_{\text{ens}}^{\min}$  required to account for the mitigated `ibm_torino` violations is not excluded by the observed nonstationarity, whereas for `ibm_fez` a local explanation would require substantially larger  $\delta_{\text{ens}}$  that is not directly witnessed by the Pauli-axis drift measurements. Hence, the CHSH data and the independent drift diagnostic together delineate a preparation-dependent loophole:  $|S| > 2$  can coexist with a breakdown of the stationarity premise required for the ideal CHSH bound.

It is instructive to compare the scale of preparation nonstationarity required here with the degree of measurement dependence invoked in Hall-type analyses. Hall showed that reproducing the quantum value  $|S| = 2\sqrt{2}$  within a local model requires measurement dependence at the level  $M \gtrsim 2(\sqrt{2} - 1)/3 \approx 0.14$ , corresponding to a  $\sim 14\%$  violation of measurement independence. By contrast, the preparation-dependent relaxation considered here requires  $\delta_{\text{ens}}^{\min} = (|S| - 2)/6$ , which corresponds to ensemble divergences of order  $\sim 3\text{--}4\%$  for the mitigated `ibm_torino` violations and  $\sim 11\text{--}12\%$  for `ibm_fez`. Although  $M$  and  $\delta_{\text{ens}}$  quantify logically distinct assumption relaxations and are not directly comparable, this contrast is informative: modest levels of preparation nonstationarity, well below the measurement-dependence scale required in Hall’s model, are sufficient to relax the Bell bound to the experimentally observed values. Importantly, unlike  $M$ , preparation nonstationarity is directly witnessed operationally on hardware through bin-resolved drift diagnostics, without invoking correlations between hidden variables and measurement choices.

To relate  $\delta_{\text{op}}$  to the CHSH aggregation actually performed, one must account for how the execution schedule samples time

across different contexts. We capture this effect through a schedule-exposure factor  $\delta_{\text{sched}}$ , which quantifies the degree of temporal separation between contexts induced by the schedule. Because  $\delta_{\text{sched}}$  controls how temporal drift is mapped into context dependence, a conservative schedule-aware lower bound on the ensemble nonstationarity entering the CHSH experiment is

$$\delta_{\text{ens}} \gtrsim \delta_{\text{sched}} \delta_{\text{op}}. \quad (13)$$

This bound is not an equality and does not purport to measure the total ensemble variation; rather, it quantifies the minimum nonstationarity that must be present in the aggregated Bell data given the observed drift and the actual execution schedule.

For round-robin execution,  $\delta_{\text{sched}} = 0$  by construction, so the schedule-induced lower bound is zero even when  $\delta_{\text{op}} > 0$ . This reflects the fact that round-robin sampling suppresses the exposure of drift in Bell aggregation without eliminating the drift itself. In contrast, for unbalanced schedules,  $\delta_{\text{sched}} \approx 1$ , yielding  $\delta_{\text{ens}} \gtrsim \delta_{\text{op}}$ . Using the experimentally observed values  $\delta_{\text{op}} \approx 0.089$  for `ibm_torino` and  $\delta_{\text{op}} \approx 0.062$  for `ibm_fez` under unbalanced execution, this establishes nonzero ensemble nonstationarity entering the corresponding CHSH tests. Using  $\underline{\delta}_{\text{ens}} \equiv \delta_{\text{sched}} \delta_{\text{op}}$  as a conservative schedule-aware lower bound, we may define a minimal relaxed bound under a LHV model.

$$S_{\text{LHV}}^{\min} = 2 + 6 \underline{\delta}_{\text{ens}} \leq 2 + 6 \delta_{\text{ens}}. \quad (14)$$

For unbalanced execution, this gives  $S_{\text{LHV}}^{\min} \approx 2.53$  on `ibm_torino` and 2.37 on `ibm_fez`. On `ibm_torino`, the mitigated CHSH value satisfies  $|S| < S_{\text{LHV}}^{\min}$ , indicating that even this conservative bound is sufficient to accommodate the observed correlations within the preparation nonstationarity loophole. In contrast, on `ibm_fez` we observe  $|S| > S_{\text{LHV}}^{\min}$  after mitigation, showing that the *minimum* relaxation implied by our bound is not, by itself, enough to account for the measured violation. This does not rule out a larger  $\delta_{\text{ens}}$  during the CHSH acquisition (e.g., axis-dependent drift or additional schedule-induced context separation), but it demonstrates that the loophole strength required to explain the `ibm_fez` data would have to exceed our conservative lower bound.

#### D. Qiskit-Aer simulations using a deterministic LHV model

To connect the experimentally observed single-channel nonstationarity (Fig. 2) to relaxed Bell bounds, we adapt a simple finite hidden-variable model from the class of deterministic, no-signalling models introduced by Hall [34]. The modification is minimal: we preserve deterministic local response functions and operational measurement independence, but allow the preparation ensemble to vary slowly in time.

We take a discrete hidden-variable space  $\Lambda = \{\lambda_1, \dots, \lambda_5\}$ , where each  $\lambda_j$  may be interpreted as an effective hardware “mode” of a given qubit pair. Local outcomes are deterministic,  $A(a, \lambda_j), B(b, \lambda_j) \in \{\pm 1\}$ , with response functions chosen as in Tab. II. For a fixed preparation ensemble, this reproduces Hall’s finite model and yields  $S = 2 + 6p$  for a suitable mixture parameter  $p$ .

TABLE II. Deterministic local response functions used in the finite hidden-variable model. Overall sign flips of  $A$  or  $B$  leave  $|S|$  invariant and are omitted.

$\lambda_j$	$A(x, \lambda_j)$	$A(x', \lambda_j)$	$B(y, \lambda_j)$	$B(y', \lambda_j)$
$\lambda_1$	+1	+1	+1	+1
$\lambda_2$	+1	-1	+1	+1
$\lambda_3$	+1	+1	+1	-1
$\lambda_4$	+1	-1	-1	+1
$\lambda_5$	+1	+1	+1	+1

TABLE III. Time-resolved preparation ensembles  $\pi_{ab}^{(k)}(\lambda_j)$  for each CHSH context  $(a, b)$ . Here  $0 \leq p_k \leq 1/3$  for all bins  $k$ . For fixed  $k$  this reduces to Hall's finite model.

	$\pi_{xy}^{(k)}$	$\pi_{x'y'}^{(k)}$	$\pi_{x'y}^{(k)}$	$\pi_{x'y'}^{(k)}$
$\lambda_1$	$p_k$	$p_k$	$p_k$	0
$\lambda_2$	$p_k$	$p_k$	0	$p_k$
$\lambda_3$	$p_k$	0	$p_k$	$p_k$
$\lambda_4$	0	$p_k$	$p_k$	$p_k$
$\lambda_5$	$1 - 3p_k$	$1 - 3p_k$	$1 - 3p_k$	$1 - 3p_k$

To model experimentally relevant drift, we introduce a discrete time (or bin) index  $k$  and allow the preparation ensemble to vary as  $\pi_{ab}^{(k)}(\lambda_j)$  according to Tab. III, with  $0 \leq p_k \leq 1/3$ . For each fixed bin  $k$ , the preparation ensemble is identical across all CHSH contexts, so that measurement independence is preserved within each bin. The Bell parameter in bin  $k$  is therefore  $S^{(k)} = 2 + 6p_k$ , and temporal variation of  $p_k$  induces bin-resolved changes in correlators without introducing context dependence at the preparation level. The operational single-channel drift is

$$\delta_{\text{op}}^{(ab)} = \max_{k, k'} d_{\text{TV}}\left(\pi_{ab}^{(k)}, \pi_{ab}^{(k')}\right) = |p_k - p_{k'}|, \quad (15)$$

directly mirroring the experimentally observed bin-to-bin variation in outcome statistics for a fixed measurement setting. Thus, nonzero  $\delta_{\text{op}}$  reflects temporal preparation nonstationarity rather than correlations between  $\lambda$  and the measurement choices.

In an actual CHSH experiment, different measurement contexts  $(a, b)$  are executed over (possibly distinct) subsets of time bins  $\mathcal{K}_{ab}$ . The effective preparation ensemble entering the Bell inequality is therefore the time-averaged mixture

$$\bar{\pi}_{ab}(\lambda_j) = \frac{1}{|\mathcal{K}_{ab}|} \sum_{k \in \mathcal{K}_{ab}} \pi_{ab}^{(k)}(\lambda_j), \quad (16)$$

with effective parameters  $\bar{p}_{ab} = |\mathcal{K}_{ab}|^{-1} \sum_{k \in \mathcal{K}_{ab}} p_k$ . The ensemble divergence relevant for the relaxed CHSH bound is

$$\delta_{\text{ens}} = \max_{(ab), (a'b')} d_{\text{TV}}(\bar{\pi}_{ab}, \bar{\pi}_{a'b'}) = \max_{(ab), (a'b')} |\bar{p}_{ab} - \bar{p}_{a'b'}|. \quad (17)$$

Crucially,  $\delta_{\text{ens}}$  can become nonzero even though the underlying mechanism is purely temporal drift within a single preparation channel. Nonuniform scheduling maps this drift onto different CHSH contexts, producing effective context-conditioned ensembles. In this sense, the experimentally observed single-channel nonstationarity  $\delta_{\text{op}} > 0$  implies that the

TABLE IV. Simulation results for the drifting finite model with initially context-independent ensembles ( $p_k \in [0, 0.15]$ ,  $K = 12$  bins, 1024 shots/bin). Balanced uses round-robin bin assignment; Unbalanced assigns early bins to  $XY/XY'$  and late bins to  $X'Y/X'Y'$ . The IID null uses constant  $p_k = 0.08$ . Values are simulation averages.

Schedule	$S_r$	$\delta_{\text{op}}$ (global)	$\delta_{\text{ens}}$
Balanced	2.090	0.334	0.124
Unbalanced	2.191	0.169	0.288
IID null	2.000	0.013	0.007

hidden variable  $\lambda$  is effectively time dependent, and scheduling converts this time dependence into context dependence at the level relevant for Bell inequalities.

To quantify this mechanism, we simulate the above model under conditions matched to the experiments. We initialize all four CHSH contexts with identical ensembles in each bin, eliminating intrinsic measurement dependence. Temporal drift is introduced via a linear ramp  $p_k \in [0, 0.15]$  over  $K = 12$  bins, comparable to the variations inferred from hardware. Monte Carlo null tests with constant  $p_k$  yield  $|S| \approx 2.00$  with small  $\delta_{\text{op}}$  and  $\delta_{\text{ens}}$  consistent with finite-shot fluctuations.

Under balanced (round-robin) scheduling, all contexts sample identical time-averaged ensembles, so  $\delta_{\text{ens}}$  remains small despite a large global  $\delta_{\text{op}}$ . By contrast, under unbalanced scheduling—where early bins preferentially contribute to  $(x, y)$  and  $(x, y')$  and late bins to  $(x', y)$  and  $(x', y')$ —the same temporal drift produces a substantial ensemble mismatch  $\delta_{\text{ens}} \sim 0.3$ , accompanied by a relaxed Bell parameter  $|S| \gtrsim 2.2$ . These values are quantitatively consistent with the mitigated experimental results for `ibm_torino` and `ibm_fez`. These simulations validate a preparation-dependent loophole on NISQ hardware. Nonzero  $\delta_{\text{op}}$  provides an operational witness of temporal nonstationarity, while scheduling amplifies this drift into effective ensemble divergences  $\delta_{\text{ens}}$  sufficient to relax the CHSH bound. Unlike Hall's original construction, no explicit correlation between hidden variables and measurement settings is introduced; nevertheless, the resulting context-conditioned ensembles occupy the same regime of relaxed Bell inequalities.

#### IV. CONCLUSION

We have investigated the role of preparation nonstationarity in Bell–CHSH experiments on superconducting quantum processors. By relaxing the assumption of a single stationary preparation ensemble—while preserving locality and measurement independence—we derived a relaxed Bell inequality,  $|S| \leq 2 + 6\delta_{\text{ens}}$ , that quantifies how ensemble divergence alone can inflate the Bell parameter. This framework isolates a preparation-dependent loophole that is logically distinct from Hall-type measurement dependence and is directly motivated by known non-i.i.d. effects in superconducting hardware.

Operationally, we introduced  $\delta_{\text{op}}$  as a witness of preparation nonstationarity, based on bin-resolved outcome statistics for fixed measurement channels. Pauli-axis measurements on `ibm_fez` and `ibm_torino` reveal statistically significant

drift exceeding matched Monte Carlo nulls, persisting after full two-qubit readout mitigation. These observations certify  $\delta_{\text{ens}} > 0$  without relying on assumptions about hidden-variable dynamics or measurement dependence. In contrast, apparent drift extracted from CHSH-optimal settings is removed by mitigation, confirming that such measurements conflate preparation drift with basis-dependent measurement instability and are unsuitable for diagnosing nonstationarity.

Although  $\delta_{\text{ens}}$  cannot be inferred directly from operational data, the observed Bell violations imply a minimal ensemble divergence  $\delta_{\text{ens}}^{\text{req}} = (|S| - 2)/6$  for any local explanation. For the qubit pairs studied here, the required divergence ranges from a few to  $\sim 10\%$ , comparable to the scale of measurement dependence invoked in Hall-type models. Simulations of a drifting finite hidden-variable model demonstrate that purely

temporal preparation drift, when combined with nonuniform scheduling, can amplify intra-context nonstationarity into effective context-dependent ensembles sufficient to relax the CHSH bound without signaling.

Taken together, these results show that Bell violations on noisy intermediate-scale quantum hardware can coexist with a breakdown of the preparation-stationarity premise underlying the ideal CHSH bound. This preparation-dependent loophole underscores the need for drift-aware experimental protocols and operational diagnostics when using Bell tests for quantum certification on real devices.

*Acknowledgments* G.S. and R. P. thank Global Initiative of Academic Networks (GIAN) and IIT Delhi, which provided the environment in which this project was conceived. G.S. acknowledges ANRF-SERB Core Research Grant CRG/2023/005628.

- 
- [1] M. Kjaergaard, M. E. Schwartz, J. Braum"uller, P. Krantz, J. I.-J. Wang, S. Gustavsson, and W. D. Oliver, *Annu. Rev. Condens. Matter Phys.* **11**, 369 (2020).
- [2] F. Arute, K. Arya, R. Babbush, D. Bacon, J. C. Bardin, R. Barends, R. Biswas, S. Boixo, F. G. S. L. Brando, D. A. Buell, B. Burkett, *et al.*, *Nature* **574**, 505 (2019).
- [3] M. Ansmann, H. Wang, R. C. Bialczak, M. Hofheinz, E. Lucero, M. Neeley, A. D. O'Connell, D. Sank, M. Weides, J. Wenner, A. N. Cleland, and J. M. Martinis, *Nature* **461**, 504 (2009).
- [4] J. M. Chow, J. M. Gambetta, A. D. Córcoles, S. J. Srinivasan, J. A. Smolin, S. Merkel, J. R. Rozen, G. A. Keefe, M. B. Rothwell, M. B. Ketchen, and M. Steffen, *Nature* **508**, 500 (2014).
- [5] C. Neill, P. Roushan, K. Kechedzhi, S. Boixo, A. Mezzacapo, B. Burkett, *et al.*, *Science* **360**, 195 (2018).
- [6] K. Bharti, A. Cervera-Lierta, T. H. Kyaw, T. Haug, S. Alperin-Lea, A. Anand, M. Degroote, H. Heimonen, J. S. Kottmann, T. Menke, *et al.*, *Reviews of Modern Physics* **94**, 015004 (2022).
- [7] J. Tilly, H. Chen, S. Cao, D. Picozzi, K. Setia, Y. Li, E. Grant, L. Wossnig, I. Rungger, G. H. Booth, *et al.*, *Physics Reports* **986**, 1 (2022).
- [8] B. Fauseweh, *Nature Communications* **15**, 2123 (2024).
- [9] C. W. Bauer, Z. Davoudi, A. B. Balantekin, T. Bhattacharya, M. Carena, W. A. De Jong, P. Draper, A. El-Khadra, N. Gemelke, M. Hanada, *et al.*, *PRX quantum* **4**, 027001 (2023).
- [10] P. Scholl, M. Schuler, H. J. Williams, A. A. Eberharter, D. Barredo, K.-N. Schymik, V. Lienhard, L.-P. Henry, T. C. Lang, T. Lahaye, *et al.*, *Nature* **595**, 233 (2021).
- [11] R. Barends, J. Kelly, A. Megrant, A. Veitia, D. Sank, *et al.*, *Nature* **508**, 500 (2014).
- [12] S. Storz, J. Sch"ar, A. Kulikov, P. Magnard, and P. e. a. Kurpiers, *Nature* **617**, 265 (2023).
- [13] J. Koch, T. M. Yu, J. Gambetta, A. A. Houck, D. I. Schuster, J. Majer, A. Blais, M. H. Devoret, S. M. Girvin, and R. J. Schoelkopf, *Phys. Rev. A* **76**, 042319 (2007).
- [14] M. A. Nielsen and I. L. Chuang, *Quantum Computation and Quantum Information* (Cambridge University Press, 2010).
- [15] A. Javadi-Abhari, M. Treinish, K. Krsulich, C. J. Wood, J. Lishman, J. Gacon, S. Martiel, P. D. Nation, L. S. Bishop, A. W. Cross, *et al.*, arXiv preprint arXiv:2405.08810 (2024).
- [16] K. Rudinger, T. Proctor, D. Langharst, M. Sarovar, K. Young, and R. Blume-Kohout, *Physical Review X* **9**, 021045 (2019).
- [17] T. J. Proctor, M. C. Revelle, E. Nielsen, K. Rudinger, D. Lobser, P. Maunz, and R. Blume-Kohout, *Nat. Commun.* **11**, 5396 (2020).
- [18] M. McEwen, D. Kafri, Z. Chen, J. Atalaya, K. Satzinger, C. Quintana, P. V. Klimov, D. Sank, C. Gidney, A. Fowler, *et al.*, *Nature communications* **12**, 1761 (2021).
- [19] W. P. Livingston, M. S. Blok, E. Flurin, J. Dressel, A. N. Jordan, and I. Siddiqi, *Nature communications* **13**, 2307 (2022).
- [20] M. Hutchings, J. B. Hertzberg, Y. Liu, N. T. Bronn, G. A. Keefe, M. Brink, J. M. Chow, and B. Plourde, *Physical Review Applied* **8**, 044003 (2017).
- [21] J. Kelly, R. Barends, A. G. Fowler, A. Megrant, E. Jeffrey, T. C. White, D. Sank, J. Y. Mutus, B. Campbell, Y. Chen, *et al.*, *Nature* **519**, 66 (2015).
- [22] J. Wenner, R. Barends, R. Bialczak, Y. Chen, J. Kelly, E. Lucero, M. Mariantoni, A. Megrant, P. O'Malley, D. Sank, *et al.*, *Applied Physics Letters* **99** (2011).
- [23] M. Howard, J. Wallman, V. Veitch, and J. Emerson, *Nature* **510**, 351 (2014).
- [24] C. Budroni, A. Cabello, O. Guhne, M. Kleinmann, and J.-Å. Larsson, *Reviews of Modern Physics* **94**, 045007 (2022).
- [25] Y. Kim, E. P. Nawrocki, J.-B. Chen, and J. e. a. Choi, *Nature* **618**, 500 (2023).
- [26] P. Zhao, *Physical Review Applied* **20**, 054033 (2023).
- [27] R. Harper, S. T. Flammia, and J. J. Wallman, *Nature Physics* **16**, 1184 (2020).
- [28] K. Goswami, C. Giarmatzi, C. Monterola, S. Shrapnel, J. Romero, and F. Costa, *Physical Review A* **104**, 022432 (2021).
- [29] D. Filenga, F. Mahlow, and F. Fanchini, *Physical Review A* **102**, 042615 (2020).
- [30] F. Setiawan, A. V. Gramolin, E. S. Matekole, H. Krovi, and J. M. Taylor, *Quantum* **9**, 1701 (2025).
- [31] J. F. Clauser, M. A. Horne, A. Shimony, and R. A. Holt, *Phys. Rev. Lett.* **23**, 880 (1969).
- [32] J. F. Clauser and M. A. Horne, *Phys. Rev. D* **10**, 526 (1974).
- [33] N. Brunner, D. Cavalcanti, S. Pironio, V. Scarani, and S. Wehner, *Rev. Mod. Phys.* **86**, 419 (2014).
- [34] M. J. Hall, *Physical review letters* **105**, 250404 (2010).
- [35] A. S. Friedman, A. H. Guth, M. J. Hall, D. I. Kaiser, and J. Gallicchio, *Physical Review A* **99**, 012121 (2019).
- [36] J. Barrett and N. Gisin, *Physical review letters* **106**, 100406 (2011).
- [37] R. Li, D. Li, W. Huang, B. Xu, and F. Gao, *Physica A: Statistical*

- Mechanics and its Applications **626**, 129037 (2023).
- [38] L. P. Thinh, L. Sheridan, and V. Scarani, arXiv preprint arXiv:1304.3598 (2013).
- [39] J. S. Bell, Physics (Long Island City, N.Y.) **1**, 195 (1964).
- [40] J.-Å. Larsson, *J. Phys. A: Math. Theor.* **47**, 424003 (2014).
- [41] G. Lima, E. Inostroza, R. Vianna, J.-Å. Larsson, and C. Saavedra, arXiv preprint arXiv:1111.0822 (2011).
- [42] R. D. Gill, *AppliedMath* **3**, 446 (2023).
- [43] D. Rosset, R. Ferretti-Schöbitz, J.-D. Bancal, N. Gisin, and Y.-C. Liang, *Physical Review A—Atomic, Molecular, and Optical Physics* **86**, 062325 (2012).
- [44] Y. Y. Gao, M. A. Rol, S. Touzard, and C. Wang, *PRX quantum* **2**, 040202 (2021).
- [45] M. Ware, G. Ribeill, D. Riste, C. A. Ryan, B. Johnson, and M. P. Da Silva, *Physical Review A* **103**, 042604 (2021).
- [46] A. Di Giovanni, A. S. Aasen, J. Lisenfeld, M. Gärttner, H. Rotzinger, and A. V. Ustinov, *Physical Review Applied* **24**, 044043 (2025).
- [47] S. Bravyi, S. Sheldon, A. Kandala, D. C. McKay, and J. M. Gambetta, *Phys. Rev. A* **103**, 042605 (2021).
- [48] S. Endo, S. C. Benjamin, and Y. Li, *Phys. Rev. X* **8**, 031027 (2018).
- [49] F. B. Maciejewski, Z. Zimborás, and M. Oszmaniec, *Quantum* **4**, 257 (2020).
- [50] F. Cosco, F. Plastina, and N. L. Gullo, arXiv preprint arXiv:2408.00869 (2024).
- [51] G. N. Tabia, A. Y.-T. Shih, J.-Y. Zheng, and Y.-C. Liang, *Quantum Science and Technology* **10**, 035056 (2025).